A NUMERICAL STRATEGY FOR RADIATIVE TRANSFER PROBLEMS WITH HIGLY OSCILLATING OPACITIES

JULIEN MATHIAUD AND FRANCESCO SALVARANI

Abstract. We propose a numerical method, suitable to study transport problems with highly oscillatory coefficients, based on a formulation of the equations in terms of a semigroup acting on an enlarged phase space. After testing the strategy on a model case, we consider the relevant situation of the radiative transfer equations.

1. Introduction

The presence of rapidly oscillating terms is one of the major difficulties when dealing with the numerical simulation of differential equations.

This problem is particularly apparent in the case of the radiative transfer, which describes, by means of a kinetic approach, a gas of photons exchanging energy with a background material (such as a plasma, a stellar or a planetary atmosphere). This energy exchange is the result of absorption, emission or scattering of photons by the atoms in the background matter. The effects of the background are described by a term, the opacity, that is in general not known explicitly, but only through tabulated values. Moreover, its dependence on the independent variables is quite involved and shows, in general, a wildly oscillating behaviour [3].

In [1], the authors explained how the notion of a "kinetic theory in extended phase space" can be used in the homogenization of the radiative transfer equation with rapidly oscillating opacities. In order to avoid the modifications of the structure of the equation caused by the homogenization limit, they proposed a new formulation of the problem in terms of a semigroup acting on an enlarged phase space (i.e. on functions involving more variables than in the original problem) which allows to keep unchanged the group properties satisfied by the solution of the equation.

In this paper we show that the strategy of [1] is useful not only from the viewpoint of semigroup theory. Indeed, it can be also the starting point for developing a new numerical strategy for some classes of transport equations with rapidly oscillating terms.

This new numerical approach has two advantages with respect to a standard discretization procedure: first of all, it is very robust with respect to the modification of the structure of the transport equations under the homogenization process.

Moreover, this strategy has the peculiar feature of transferring the effects of the fast oscillations from the equations to the initial data only. As a

Key words and phrases. Homogenization, Radiative transfer, Opacities.

consequence, the homogenization with respect to the fast oscillating scale is performed only once, at the beginning of the numerical procedure.

The paper is organized as follows: in the next section we consider, on a theoretical example, the homogenization effect on the structure of an ordinary differential equation and test our strategy on this model problem. Finally, in Section 3, we apply our method to a radiative transfer problem, which is a natural framework where rapidly oscillating terms can modify the structure of the limit equations.

2. A model problem

2.1. **The problem.** Our starting point is the following example, due to L. Tartar [5]. It shows that the the homogenization of some evolutionary differential equations may lead to evolution problems with a completely different structure, usually integro-differential equations with memory effects.

Let $a \in L^\infty(\mathbb{T}^N)$, with $a \geq 0$ a.e. on $\mathbb{T}^N$, and consider, for each $\epsilon > 0$, the ODE with unknown $u_\epsilon \equiv u_\epsilon(t,z) \in \mathbb{R}$:

$$\begin{cases} \dfrac{du_\epsilon}{dt} + a\left(\dfrac{z}{\epsilon}\right) u_\epsilon = 0, \quad t > 0,\ z \in \mathbb{R}^N, \\ u_\epsilon(0,z) = u^{in}(z), \end{cases} \tag{2.1}$$

where $u^{in} \in L^2(\mathbb{R}^N) \cap L^\infty(\mathbb{R}^N)$.

It is well known that this problem admits the explicit solution

$$u_\epsilon(t,z) = u^{in}(z) e^{-ta(z/\epsilon)}, \quad t > 0,\ z \in \mathbb{R}^N,$$

for each $\epsilon > 0$.

In the limit as $\epsilon \to 0^+$, we obtain

$$u_\epsilon \rightharpoonup u \text{ in } L^\infty(\mathbb{R}_+ \times \mathbb{R}^N) \ \text{ weak-*}$$

where the limit u is explicitly given by the formula

$$u(t,z) = u^{in}(z)\Phi(t), \quad t \geq 0,\ z \in \mathbb{R}^N, \tag{2.2}$$

with

$$\Phi(t) = \int_{\mathbb{T}^N} e^{-ta(y)} dy\,, \quad t \geq 0. \tag{2.3}$$

It is apparent that the homogenized solution u does not satisfy the equation

$$\begin{cases} \dfrac{du}{dt} + \overline{a} u = 0, \quad t > 0,\ z \in \mathbb{R}^N, \\ u_\epsilon(0,z) = u^{in}(z), \end{cases} \tag{2.4}$$

where $\overline{a}$ is the average of a on $\mathbb{T}^N$, i.e.

$$\overline{a} = \int_{\mathbb{T}^N} a(y) dy.$$

Indeed, as shown by Tartar, the homogenized solution satisfies the following integro-differential equation

$$\begin{cases} \dfrac{du}{dt}(t,z) + \overline{a} u(t,z) = \displaystyle\int_0^t K(t-s) u(s,z) ds\,, \quad t > 0\,,\ z \in \mathbb{R}^N\,, \\ u(0,z) = u^{in}(z)\,, \end{cases} \tag{2.5}$$

where the Laplace transform of K is given by the expression

$$\tilde{K}(p) := \int_0^\infty e^{-pt} K(t)dt = \int_{\mathbb{T}^N} (p+a(y))dy - \left(\int_{\mathbb{T}^N} \frac{dy}{p+a(y)} dy \right)^{-1}, \quad p > 0\,.$$

2.2. **The theoretical background.** A difficult point for the numerical simulations is given by the oscillations of the function a with respect to the space variable z. The space variable is not influenced by the differential operator: this fact is the responsible of the modification of the structure of the equation through the homogenization process.

The theoretical basis of our strategy is given by the following proposition, whose proof has been given in [1].

Proposition 2.1. *Let $a_\epsilon \equiv a_\epsilon(z)$ be a bounded family of functions in $L^\infty(\mathbb{R}^N)$ converging in the sense of Young measures to $(\mu_z)_{z\in\mathbb{R}^N}$ and $a \in L^\infty(\mathbb{T}^N)$, with $a \geq 0$ a.e. on $\mathbb{T}^N$. Let moreover u_ϵ be the solution of the Cauchy problem (2.1) for each $\epsilon > 0$.*

Then, in the limit as $\epsilon \to 0^+$, one has

$$u_\epsilon \rightharpoonup u = \int_0^{+\infty} U ds \ \text{in } L^\infty(\mathbb{R}_+ \times \mathbb{R}^N) \text{ weak-}*,$$

where $U \equiv U(t, s, z)$ is the solution of

$$\begin{cases} \partial_t U - \partial_s U = 0\,, \quad t, s > 0\,,\ z \in \mathbb{R}^N\,, \\ U(0, s, z) = -u^{in}(z) \dfrac{d\tilde{\mu}_z}{ds}(s) \end{cases} \tag{2.6}$$

and $\tilde{\mu}_z$ is the Laplace transform of μ_z.

As already pointed out in the introduction, this result has the great advantage to transfer the effects of the fast oscillations on the initial data, and it allows to keep unchanged the structure of the equation, even when performing the limiting procedure as $\epsilon \to 0^+$.

2.3. **The numerical strategy.** The numerical method for solving the problem consists in discretizing Equation (2.6) instead of considering Equation (2.1). We work hence in the phase space individuated by the variables (z, s).

We define on the spatial domain of the equation, described by the variable z, a regular Cartesian grid, $(z_j)_{0\leq j\leq J}$ with $J \geq 1$. We set $\Delta z = 1/J > 0$, so that we have $z_j = j\Delta z$. In order to filter the rapid oscillations of the initial data of Equation (2.6), we apply a strategy, theoretically studied in [2], which consists in averaging many sampling of the initial condition, assessed on random points of each interval $[z_j, z_{j+1}]$, such points being distributed with an uniform law.

Then, the numerical solution of (2.6) is obtained by applying to this filtered initial data the transport operator, which can be numerically treated by means of a standard finite-differences non-oscillatory method (see [4]).

Finally, the solution of Equation (2.1) is obtained by integrating, with respect to the scalar supplementary variable s, the numerical solution of (2.6) by means of a standard quadrature rule. We point out that the solution of (2.6) is essentially a Laplace transform (see [1]), hence the contributions to the integral for large values of s are negligible.

Our method is robust with respect to the homogenization procedure and to the changes in the structure of the equation caused by the homogenization process. Indeed, in the enlarged phase space, the structure of Equation (2.6) is independent of ϵ, and the effects of the fast oscillations are transferred from the equations on the initial data only. The homogenization of the initial condition with respect to the fast oscillating parameter is performed only once, at the beginning of the simulation.

2.4. **Numerical simulations.** We now implement the strategy explained before and describe some relevant numerical tests.

Preliminarily, it is to point out that the error that can be performed by considering the Cauchy problem (2.4) as the limit of Equation (2.1) is not negligible. In Figure 1 we give an example of the error committed by replacing the solution of the Cauchy problem (2.5) with the naive approximation of Equation (2.1) given by the solution of (2.4). The initial datum is $u^{in}(z) = \sin(z)/(1 + z^2)$ and both solutions have been computed at time $t = 0.4$.

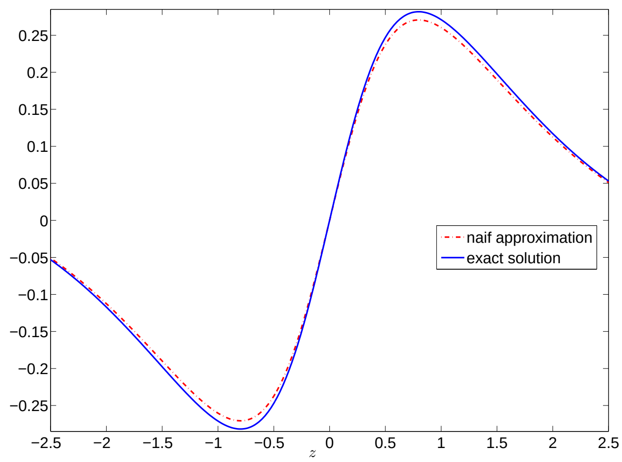

FIGURE 1. Comparison between the solution of the homogenized problem (2.5) (continuous blue line) and the naive approximation given by the solution of the Cauchy problem (2.4) (dotted red line) at time $t = 0.4$.

Moreover, we note that, even when the relaxation parameter ϵ is not too small, the solution of the homogenized problem already looks as the correct weak-* limit of the solution of the Cauchy problem (2.1).

In order to emphasize the homogenization effect, we compare in Figure 2 the solution of (2.1), with $\epsilon = 0.1$, with initial datum $u^{in}(z) = \sin(z)/(1+z^2)$ and the solution of the homogenized problem (2.5), with the same initial data, at time $t = 0.4$.

In the numerical examples described below, we use Equation (2.6) in order to obtain the numerical solution of Equation (2.1).

The numerical values of the supplementary variable s have been reduced to the interval $[0, 5]$, instead of belonging to the whole positive part of the real axis.

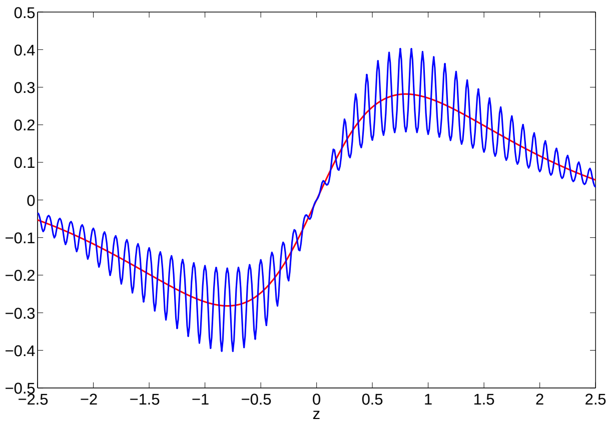

FIGURE 2. Comparison between the solutions of (2.1) (blue line) and of (2.5) (red line) at time $t = 0.4$.

Indeed, we have numerically checked that greater values of s do not give a substantial contribution to the reconstruction of the numerical solution of problem (2.1), obtained by integrating the solution of (2.6) with respect to s on its whole domain of definition. This happens because the effect of the exponential function in the definition of the Laplace transform is very dominant in the computation of the integral. The interval of definition of s has been divided in $6/\Delta t$ sub-intervals, the time step being $\Delta t = 0.05$.

We have supposed here that $z \in [0, 1]$. The initial condition of Equation (2.1) is $u^{in}(z) = z(1 - z)$ and the decay rate is $a(z) = \cos(2z/\epsilon)/4 + 1$, with $\epsilon = 10^{-6}$.

In Figures 3 and 4 we compare the exact solution of the Cauchy problem (2.5) (dotted blue line), the numerical solution of Equation (2.1), without any filter on the high frequencies (continuous red line), and the numerical solution of the reconstruction based on the integration of the solution of Equation (2.6) with respect to the supplementary variable s.

The quadrature method used here is a standard trapezoidal rule. In this latter case, the initial condition has been the result of 100 samples of u^{in} (continuous violet line). All the tests have been performed at time $t = 1$.

It is apparent that, while a standard discretization strategy does not give results which are close to the weak-* limit of the solution of (2.1) for small values of ϵ, our method gives an accurate reconstruction of the solution, which is close to the analytical solution of Equation (2.5).

On the other hand, our strategy gives a reasonably accurate result even for numerical values of $\epsilon \gg 0$.

In Figure 5 we compare the exact solution of Equation (2.1) and the reconstruction given by our method when $\epsilon = 1$ at time $t = 1$. Again, $z \in [0, 1]$, the initial condition is $u^{in}(z) = z(1 - z)$ and the decay rate is $a(z) = \cos(2z/\epsilon)/4 + 1$.

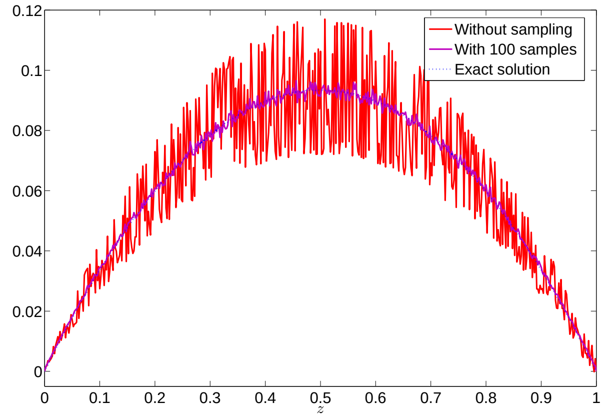

FIGURE 3. Comparison between the exact solution of the Cauchy problem (2.5), the numerical solution of Equation (2.1) and the numerical solution based on Equation (2.6).

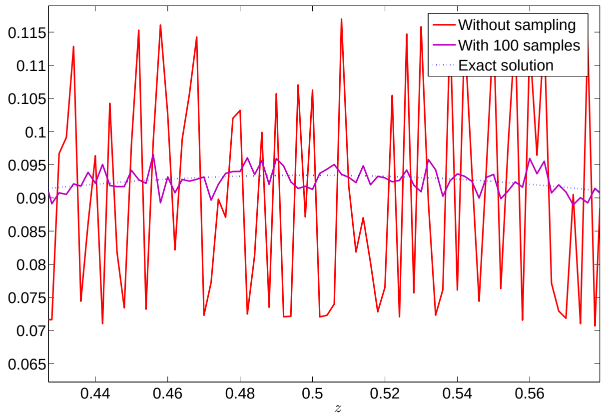

FIGURE 4. Zoom on Figure 3.

3. The radiative transfer equation

We apply now the method described in the previous section to a more complicated problem, which arises in the study of radiative transfer.

3.1. **The problem.** The state at time t of the population of photons is given by the specific radiative intensity $I(t, x, \omega, \nu)$ that is $ch\nu$ times the number density of photons with frequency ν located at the position x with direction ω. Here, h is Planck's constant, while c is the speed of light.

If we neglect scattering phenomena, the radiative intensity satisfies the radiative transfer equation

$$\frac{1}{c}\partial_t I + \omega \cdot \nabla_x I = \sigma(\nu, T)B_\nu(T) - \sigma(\nu, T)I \,. \tag{3.1}$$

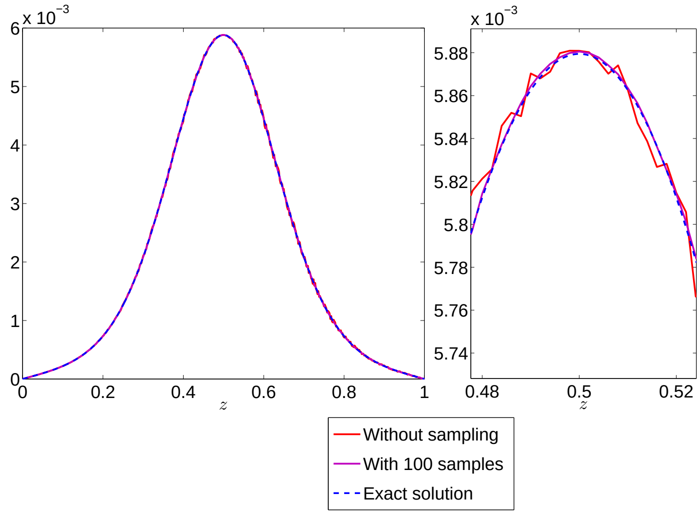

FIGURE 5. Comparison between the exact solution of (2.1) and the reconstruction given by our method in the case $\epsilon = 1$.

Here $B_\nu(T)$ is the specific radiative intensity at frequency ν of a black body at temperature T, while $\sigma(\nu, T) > 0$ is the opacity of the background material at temperature T for an incident radiation with frequency ν. While $B_\nu(T)$ has the explicit expression

$$B_\nu(T) = \frac{2h\nu^3}{c^2} \frac{1}{e^{h\nu/kT} - 1} ,$$

the opacity $\sigma(\nu, T)$ is in general not known explicitly but tabulated. Moreover, the dependence of $\sigma(\nu, T)$ in ν and T is quite involved, and the function $\nu \mapsto \sigma(\nu, T)$ can be wildly oscillating, as shown in [3].

We recognize in (3.1) the same type of behaviour of the model problem described in Section 3, since the oscillations in the opacity $\sigma(\nu, T)$ are due to the dependence on the frequency ν, while the streaming operator $(c^{-1}\partial_t + \omega \cdot \nabla_x)$ acts on the variables t and x only.

Once assumed that the temperature $T \equiv T(t, x)$ is given in the background medium which occupies the Euclidian space $\mathbb{R}^3$, the radiative transfer equation can be written under the form

$$\begin{cases} \dfrac{1}{c}\partial_t I_\epsilon + \omega \cdot \nabla_x I_\epsilon = \sigma_\epsilon(\nu, T) B_\nu(T) - \sigma_\epsilon(\nu, T) I_\epsilon \,, \\ I_\epsilon\big|_{t=0} = I^{in}(x, \omega, \nu) \,, \end{cases} \tag{3.2}$$

posed for $(t, x, \omega, \nu) \in \mathbb{R}_+^* \times \mathbb{R}^3 \times \mathbb{S}^2 \times \mathbb{R}_+^*$. Here the oscillations of the opacity are recorded by the small parameter ϵ that is the typical "oscillation wavelength" in the variable ν.

3.2. **The theoretical background.** The difficult point for the numerical simulations is given by the rapid oscillations of the opacity $(\sigma_\epsilon(\nu, T))_{\epsilon > 0}$, governed by the small parameter ϵ.

In order to overcome this difficulty, we can apply the strategy described in the previous section. By working in an enlarged phase space, we will obtain an equivalent formulation of the problem, whose structure is independent of the homogenization process and which transfers the oscillations on the initial conditions only.

The following theorem, proved in [1], is the main tool of our numerical study of the problem:

Theorem 3.1. *Let us assume that $T \in [\theta, \Theta]$ for some constants $0 < \theta < \Theta$, and that the family $(\sigma_\epsilon(\nu, T))_{\epsilon>0}$ satisfies the uniform bound*

$$0 < m \le \sigma_\epsilon(\nu, T) \le M\,, \qquad \text{for each } \epsilon, \nu > 0 \text{ and } T \in [\theta, \Theta].$$

Moreover, let us suppose that, for each $T > 0$, the family $\sigma_\epsilon(\cdot, T)$ converges in the sense of Young measures to $(\mu_\nu^T)_{\nu>0}$ as $\epsilon \to 0^+$.

Then, in the limit as $\epsilon \to 0^+$, one has

$$I_\epsilon \rightharpoonup I = \int_0^{+\infty} J ds \text{ in } L^\infty(\mathbb{R}_+ \times \mathbb{R}^3 \times \mathbb{S}^2 \times \mathbb{R}_+) \text{ weak-}*,$$

where $J \equiv J(t, s, x, \omega, \nu)$ is the solution of

$$\begin{cases} \dfrac{1}{c}\partial_t J + \omega \cdot \nabla_x J - \partial_s J = \dfrac{d^2 \tilde{\mu}_\nu^T}{ds^2} B_\nu(T)\,, \\ J\Big|_{t=0} = -I^{in}(x, \omega, \nu)\dfrac{d\tilde{\mu}_\nu^T}{ds}(s)\,, \end{cases} \tag{3.3}$$

posed for $(t, s, x, \omega, \nu) \in \mathbb{R}_+^* \times \mathbb{R}_+^* \times \mathbb{R}^3 \times \mathbb{S}^2 \times \mathbb{R}_+^*$, where the notation $\tilde{\mu}_\nu^T$ denotes the Laplace transform of μ_ν^T.

3.3. **The numerical strategy.** Theorem 3.1 gives the theoretical basis of our numerical strategy: instead of discretizing Equation (3.2), we discretize Equation (3.3), by working in the phase space individuated by the variables (s, x, ω, ν).

The second step consists in producing, on the interval of definition of the variable ν, a regular Cartesian grid, $(\nu_j)_{0\le j\le J}$ with $J \ge 1$. We fix $\Delta\nu > 0$, so that we have $\nu_j = j\Delta\nu$. In order to filter the rapid oscillations of the initial data in Equation (3.2), we have applied the same strategy used to filter the initial data in Equation (2.6).

Then, the numerical solution of (3.3) can be obtained by the numerical integration of the transport-like equation by means of any method for such kind of problems.

Finally, the solution of Equation (3.2) is obtained by the numerical integration of the numerical solution of (3.3), with respect to the scalar supplementary variable s. Also in this case, the solution of (3.3) is essentially a Laplace transform, hence the contributions to the integral for large values of s are negligible.

The considerations pointed out in Section 2, about the robustness of the method with respect to the homogenization procedure, are valid also in this case.

3.4. **Numerical simulations.** We now describe our numerical tests on the radiative transfer equations described at the beginning of this section. For a better readability of the figures, we have chosen to implement the one-dimensional spatial case (that is, we work in a three-dimensional phase space described by the variables (x, ν, s)), but the method works also in higher dimensions (of course, the computational cost increases proportionally to the dimension, but the conceptual framework remains unchanged).

In Figures 6 and 7 we compare the asymptotic exact solution of the Cauchy problem (3.2) (dotted blue line), with the numerical asymptotic solution of the same equation, obtained by using a standard method for transport equations, without any filter on the high frequencies (continuous red line), and the numerical solution of the reconstruction based on the integration of the solution of Equation (3.3) with respect to the supplementary variable s.

Since the angular variable ω acts only as a parameter in Equation (3.2), we have considered a spatially coherent beam, which results in choosing a particular angular direction, here $\omega = 0.5$.

Moreover, since the stationary solution does not depend on the space variables, Figures 6 and 7 have the same form for any spatial points of the domain. The frequency variable ν belongs to the interval $[0, 10]$, whereas the numerical range of the supplementary variable s has been reduced to the interval $[0, 5]$, which has been subdivided in $4/\Delta t$ sub-intervals, the time step being $\Delta t = 0.05$.

In the numerical examples described below, we have chosen the initial condition $I^{in}(x, \omega, \nu) = \nu e^{-\nu}$ and the cross section $\sigma_\epsilon(\nu) = 5(1 + 0.9\cos(2\nu/\epsilon)$, with $\epsilon = 10^{-3}$.

We have moreover chosen to scale the physical constants, in such a way that $h = c^2/2$ and $T = c^2/2k$, which means that the expression of Planck's law is simply $B_\nu = \nu^3/(e^\nu - 1)$.

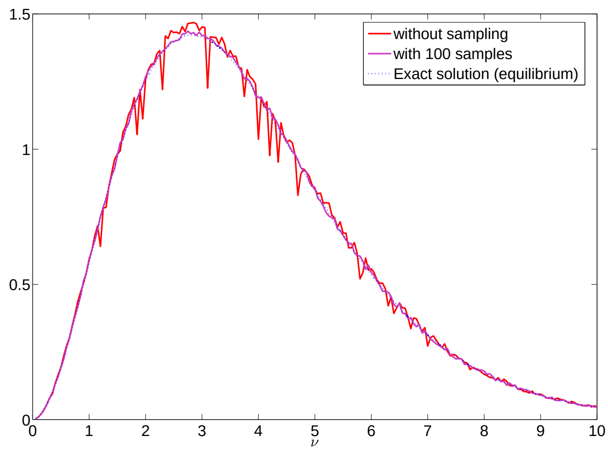

FIGURE 6. Comparison between the exact asymptotic solution of the Cauchy problem (3.2), the numerical solution of the same equation without filtering the high frequencies and the numerical solution based on the new formulation (3.3).

Also in this case, the robustness of our strategy with respect to the homogenization procedure is numerically observed.

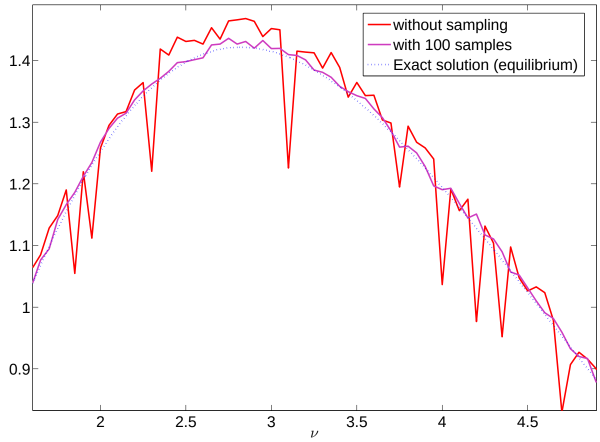

FIGURE 7. Zoom on Figure 6.

REFERENCES

[1] E. Bernard, F. Golse, F. Salvarani: Homogenization of transport problems and semi-groups; Math. Meth. in Appl. Sci., **33** (2010), 1228–1234

[2] B. Engquist, J-G Liu: Numerical methods for oscillatory solutions to hyperbolic problems; Comm. Pure Appl. Math., **46** (1993), 1327-1361

[3] C.A. Iglesias, V. Sonnad, B.G. Wilson, J.I. Castor: Frequency dependent electron collisional widths for opacity calculations; High Energy Dens. Phys. **5** (2009), 97–104.

[4] R.J. LeVeque: *Numerical methods for conservation laws. Second edition*; Lectures in Mathematics ETH Zürich, Birkhäuser Verlag, Basel, 1992.

[5] L. Tartar: *An Introduction to Navier-Stokes Equation and Oceanography*; Lecture Notes of the Unione Matematica Italiana 1, Springer, Berlin, Heidelberg, New-York, 2006.

J.M.: CEA, DAM, DIF, F-91297 ARPAJON, FRANCE & CMLA, ENS CACHAN, CNRS, UNIVERSUD, 61 AVENUE DU PRÉSIDENT WILSON, F-94230 CACHAN, FRANCE

E-mail address: `julien.mathiaud@cea.fr`

F.S.: DIPARTIMENTO DI MATEMATICA F. CASORATI, UNIVERSITÀ DEGLI STUDI DI PAVIA, VIA FERRATA 1, I-27100 PAVIA, ITALY

E-mail address: `francesco.salvarani@unipv.it`